Letters

An Optimal Damping Design of Virtual Synchronous Generators for Transient Stability Enhancement

Xiaoling Xiong, *Member, IEEE*, Chao Wu, *Member, IEEE*, Peng Cheng, *Member, IEEE*, and Frede Blaabjerg, *Fellow, IEEE*

***Abstract*— A transient damping method (TDM), introducing the frequency of a virtual synchronous generator through a high-pass filter (HPF) to the power reference, is usually adopted to stabilize the system against disturbances. However, different from a small-signal stability perspective, this letter reveals that the gain of HPF should not be too large due to the transient stability issues. Thus, an optimal parameter design method of the TDM is proposed for the improvement of transient stability. The experimental results validate the theoretical findings.**

***Index Terms*—Damping, high-pass filter (HPF), transient stability, virtual synchronous generators (VSGs).**

I. Introduction

OVER the past decade, the virtual synchronous generators (VSGs) concept was proposed to emulate the swing equation of a synchronous generator (SG) in the control of power converters [1], [2]. Consequently, the VSG can benefit from the advantages of SG, such as providing an inertial response, operating in both grid-connected, and islanded modes without changing control strategies. Thus, the VSG with short-term energy storage to provide inertia support is becoming an attractive approach for integrating renewable power into the grid. However, the emulation of the swing equation also introduces the oscillatory mode of a typical SG. Therefore, a proper damping method should be added to the VSG control.

The damping methods can be generally divided into two types. The dominant one is to add the damping effect through the active power control loop (APCL) [2]–[8], and the other is to model the damping effect via the reactive power control loop (RPCL) [9]. The simplest way is using the frequency difference between the VSG frequency and the nominal frequency in APCL, which is also known as *P–f* droop gain [2]. However, strengthening the damping effect may change the droop characteristics. To solve this problem, using the measured grid frequency to replace the nominal frequency is proposed in [3] and [4]. This method just provides a damping effect during the transient period but does not affect steady-state characteristics. However, the frequency estimator must be adopted to measure the grid frequency. To avoid using the measurement-based frequency estimator, a simpler implementation is used to replace the frequency estimator in [5] and [6], where the grid frequency can be approximated by filtering the VSG frequency with a low-pass filter (LPF). Here, the damping effect can be equivalently achieved by introducing the VSG frequency through a high-pass filter (HPF) to the active power reference, which is regarded as the transient damping method (TDM).

More damping methods with higher order filters are also proposed, i.e., the damping correction loop method [7], the state feedback with an LPF [8], using a similar conventional power system stabilizer [9], etc. However, the dynamics are becoming more complicated, and tuning the parameters of the required higher order filters is much more difficult. By comparison, the TDM through an HPF is an effective and more straightforward solution, which is our concern in this letter.

In the existing research, the parameters of TDM were just studied and designed using eigenvalue analysis from a small-signal stability perspective [5], [6]. However, the effects of TDM on transient stability when the system is subjected to a large disturbance and parameter design based on transient stability are still absent. Thus, this letter attempts to fill this gap. First, the dynamics of the transient damping term are deduced based on the power angle and the VSG frequency. Then, combining with the outer power control loops, a third-order nonlinear state-space model is derived to represent the dynamics of the system. The transient stability of the VSG is assessed by the trajectories in the state space, which reveals that the TDM has a critical impact on the transient stability. The parameter design guidelines are given based on transient responses, which are further verified by the experimental results.

Manuscript received January 8, 2021; revised February 22, 2021 and March 31, 2021; accepted April 12, 2021. Date of publication April 19, 2021; date of current version June 30, 2021. This work was supported in part by the National Natural Science Foundation of China under Grants 51707065 and 51807182 and in part by the Velux Foundations under the Villum Investigator Grant Repeps under Award 00016591. *(Corresponding author: Chao Wu.)*

Xiaoling Xiong and Peng Cheng are with the State Key Laboratory of Alternate Electrical Power System With Renewable Energy Sources, North China Electric Power University, Beijing 102206, China (e-mail: xiongxl1102@ncepu.edu.cn; p.cheng@ncepu.edu.cn).

Chao Wu and Frede Blaabjerg are with the Department of Energy Technology, Aalborg University, 9220 Aalborg, Denmark (e-mail: cwu@et.aau.dk; fbl@et.aau.dk).

Color versions of one or more figures in this article are available at https://doi.org/10.1109/TPEL.2021.3074027.

Digital Object Identifier 10.1109/TPEL.2021.3074027

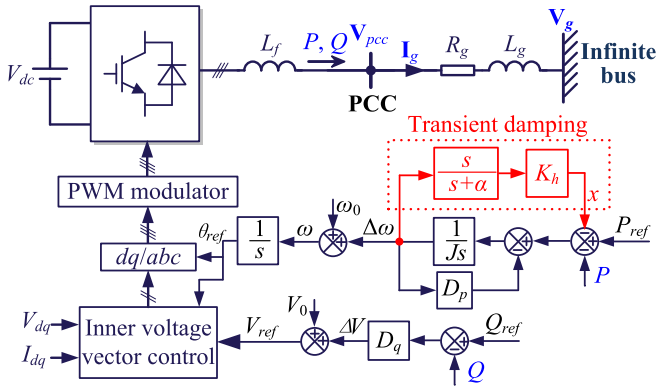

Fig. 1. General control scheme of a three-phase grid-connected VSG with the transient damping control.

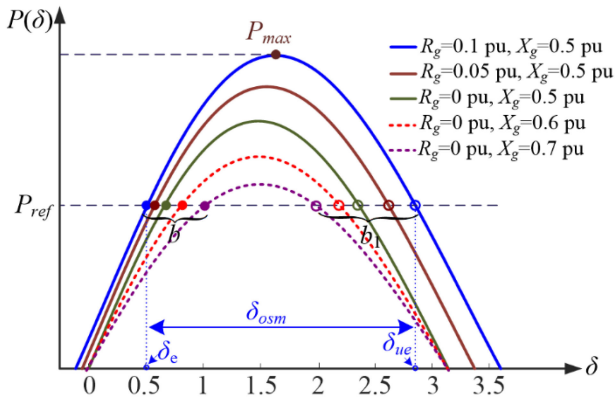

Fig. 2. $P-\delta$ curves with different R_g and X_g, the other parameters are the same as in Table I.

II. Dynamic Representation of the VSG

A. System Description

Fig. 1 shows the diagram of a grid-connected VSG with TDM, where L_f is the converter filter, L_g and R_g compose the grid impedance. $V_g = V_g e^{jw_g t}$ and V_{pcc}=$V_{pcc}e^{j\theta_{pcc}}$ are the space vectors of the grid voltage and the PCC voltage. $\boldsymbol{I}_g$ denotes the current space vector injected into the grid. P and Q represent the active and reactive power injected into the grid from the PCC. Usually, the dc-link voltage is regulated by a front-end converter [10] or by an energy storage converter [11]. Hence, a constant dc-link voltage is assumed in this letter [12], [13]. The outer power control loop, i.e., the VSG control, is to generate the PCC voltage reference, i.e., V_{ref}=$V_{ref}e^{j\theta_{ref}}$. Usually, a fast inner voltage-vector control is employed [12], [13], resulting in $\mathbf{V}_{\rm pcc}$ ideally tracking $\mathbf{V}_{\rm ref}$. Thus, $\mathbf{V}_{\rm pcc} = \mathbf{V}_{\rm ref}$.

In Fig. 1, $P_{\rm ref}$ and $Q_{\rm ref}$ are active and reactive power references. ω denotes the VSG frequency, and $\omega = \omega_0 + \Delta\omega$, which can be derived as

$$\omega = \omega_0 + \frac{1}{Js + D_p} \cdot (P_{ref} - P - x) \tag{1}$$

where J and D_p are the virtual inertia and the P–f droop gain, respectively. x denotes the HPF output term, which is derived as

$$x = \frac{K_h s}{s + \alpha}\Delta\omega. \tag{2}$$

Here, x can be divided into two parts, given as

$$x = K_h\Delta\omega - \frac{K_h\alpha}{s + \alpha}\Delta\omega \overset{\text{define}}{=} x_1 + x_2. \tag{3}$$

It can be seen that x_1 is similar to D_p term, which can provide a damping effect on the system. Without HPF ($\alpha = 0$), K_h changes the P–f droop gain, which can be entirely avoided by using an HPF to filter out the steady-state offset in $\Delta\omega$. However, the cutoff frequency of HPF should not be too large, and K_h is required to be large enough in order for the damping design to obtain the small-signal stability.

The $Q-V$ droop control is employed for the RPCL, and the control law of which is given by

$$V_{ref} = V_0 + D_q\,(Q_{ref} - Q) \tag{4}$$

where K_q is $Q-V$ droop gain and V_0 is the rated voltage magnitude.

δ is defined as the power angle, given as $\delta = \theta_{\rm ref} - \omega_g t$. Thus, P and Q can be deduced as

$$P = \frac{3}{2} \cdot \frac{\left(V_{pcc}^2 - V_{pcc}V_g cos\delta\right) R_g + X_g V_{pcc} V_g \sin\delta}{R_g^2 + X_g^2} \tag{5}$$

$$Q = \frac{3}{2} \cdot \frac{\left(V_{pcc}^2 - V_{pcc}V_g cos\delta\right) X_g - R_g V_{pcc} V_g \sin\delta}{R_g^2 + X_g^2}. \tag{6}$$

Substituting (6) into (4) and considering $V_{\rm pcc} = V_{\rm ref}$, $V_{\rm pcc}$ can be solved as a function of δ, denoted as $V_{\rm pcc}(\delta)$. Then, substituting $V_{\rm pcc}(\delta)$ into (5), the $P-\delta$ relationship when considering the effects of the RPCL, represented by $P(\delta)$, can be obtained. Thus, the $P-\delta$ curves with different R_g and X_g can be plotted, as shown in Fig. 2. It can be seen that the power transfer capability of the VSG varies with different grid impedances. The maximum power $P_{\rm max}$ that can be transmitted becomes higher with a larger R_g and smaller X_g. Meanwhile, the allowed variation range of δ, i.e., $\delta_{\rm osm}$, is much wider with a larger R_g and smaller X_g, benefiting the transient stability during grid voltage sag.

B. Dynamic Representations

The transient stability is the ability of the VSG to maintain synchronization with the grid when subjected to a large disturbance. Thus, the dynamic response of the power angle δ determines the transient stability during the grid fault, such as grid voltage sag. $\delta = \int\omega dt - \omega_g t$, where ω can be modeled with (1) under the condition that the overcurrent protection is not triggered during the grid fault. Otherwise, the VSG control should be switched to grid-following control, whose transient stability is mainly determined by PLL. Thus, this letter only focuses on the effects of TDM on transient stability without triggering the overcurrent limit.

For the conventional VSG, applying the derivation on both δ and ω, the dynamics of δ can be obtained. Different from that, the dynamics of x need to be considered when TDM is used. Therefore, the dynamic behaviors of the system in Fig. 1 can

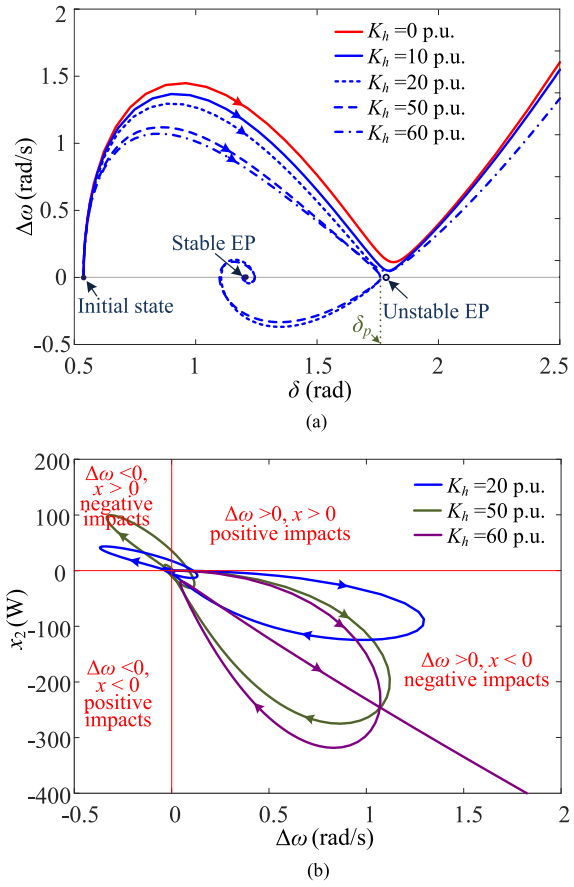

Fig. 3. Trajectories of the VSG in the state space with different K_h ($\alpha = 3$ rad/s) when the grid voltage drops from 1 to 0.6 p.u. (a) Trajectory projections on the $\Delta\omega$-δ plane, and (b) Trajectory projections of three cases on the x_2-$\Delta\omega$ plane.

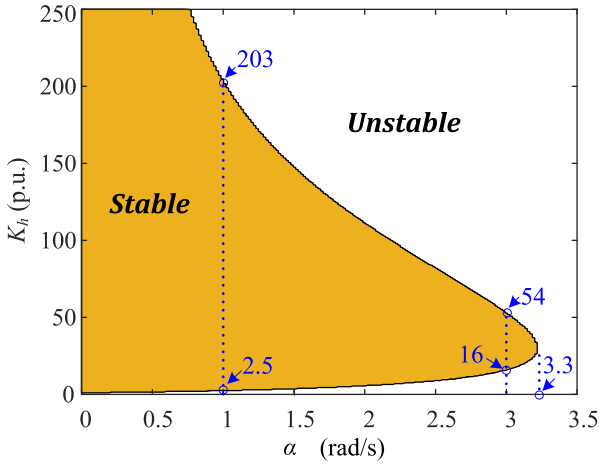

Fig. 4. Allowable range for the parameters using TDM.

be derived from (1) and (2), which is a third-order nonlinear system, represented in the standard form as

$$\begin{bmatrix} d\delta/dt \\ d\Delta\omega/dt \\ dx/dt \end{bmatrix} = \begin{bmatrix} \Delta\omega+\omega_0-\omega_g \\ (-D_p\Delta\omega + P_{ref} - P(\delta) - x)/J \\ K_h(-D_p\Delta\omega + P_{ref} - P(\delta) - x)/J - \alpha x \end{bmatrix}. \quad (7)$$

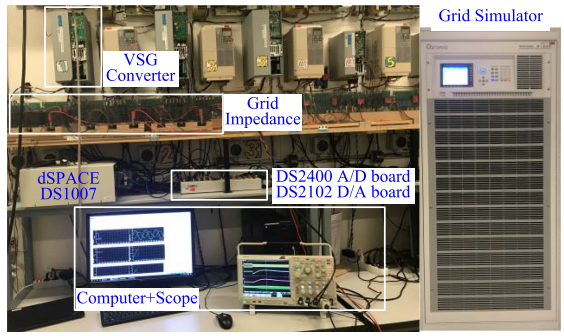

Fig. 5. Experimental setup used in the experiments.

TABLE I
MAIN PARAMETERS OF THE VSG SYSTEM USED IN EXPERIMENTS

Parameters	Description	Value	p.u.
P_{ref}	Rated active power	2 kW	1.0
Q_{ref}	Rated reactive power	0	0
V_0	Rated voltage	100 V	1.0
V_g	Normal grid voltage	100 V	1.0
ω_0	Grid angular frequency	314 rad/s	1.0
L_g	Grid inductance	12 mH	0.5
R_g	Equivalent grid resistance	48 mΩ	0.006
D_p	P-f droop gain	25 $P_{\max}/\omega_0$	25
J	Virtual inertia	20 $P_{\max}/\omega_0$	20
D_q	Q-V droop gain	0.1 $V_0/Q_{\max}$	0.1
K_h	Gain of TDM	1 $P_{\max}/\omega_0$	1

By setting all the differential items in (7) to zero, the equilibrium point (EP) $\boldsymbol{x_e} = [\delta_e, \Delta\omega_e, x_e]^T$ can be obtained. This implies $\Delta\omega_e = \omega_g - \omega_0$, $x_e = 0$, and δ_e should satisfy that $P(\delta_e) = P_{\text{ref}} - D_p(\omega_g - \omega_0)$, where two values can be solved for δ_e. The smaller δ_e is for the stable EP, and the larger one is for the unstable EP. The precondition for transient stability is that EPs exist after the grid voltage sag [12]. In order to focus on the impacts of TDM on transient stability, the grid voltage dropping from 1 to 0.6 p.u. is chosen in this letter to demonstrate the existence of EPs.

III. TRANSIENT STABILITY ANALYSIS OF VSG

A. The Impacts of TDM on Transient stability

To investigate the transient stability of the VSG, a MATLAB command "ode45" is adopted to solve the nonlinear differential equations in (7) with the steady state before the fault serving as the initial state. Thus, the solutions of the state variables in (7) can be obtained, according to which the state-space trajectories after grid voltage sag can be plotted. To provide more clear visual support, the trajectory projections on the $\Delta\omega$-δ plane are preferably used instead of the three-dimensional state-space, as shown in Fig. 3(a), where the main parameters in Table I are used. From Fig. 3(a), the responses of δ and $\Delta\omega$ after the grid voltage sag can be intuitively observed. δ increases when $\Delta\omega > 0$, and decreases when $\Delta\omega < 0$. If $\Delta\omega$ fails to decline to zero before the unstable EP, δ will diverge to infinite, which would cause instability, such as the control without TDM ($K_h = 0$). The TDM with a proper coefficient K_h can remove the instability

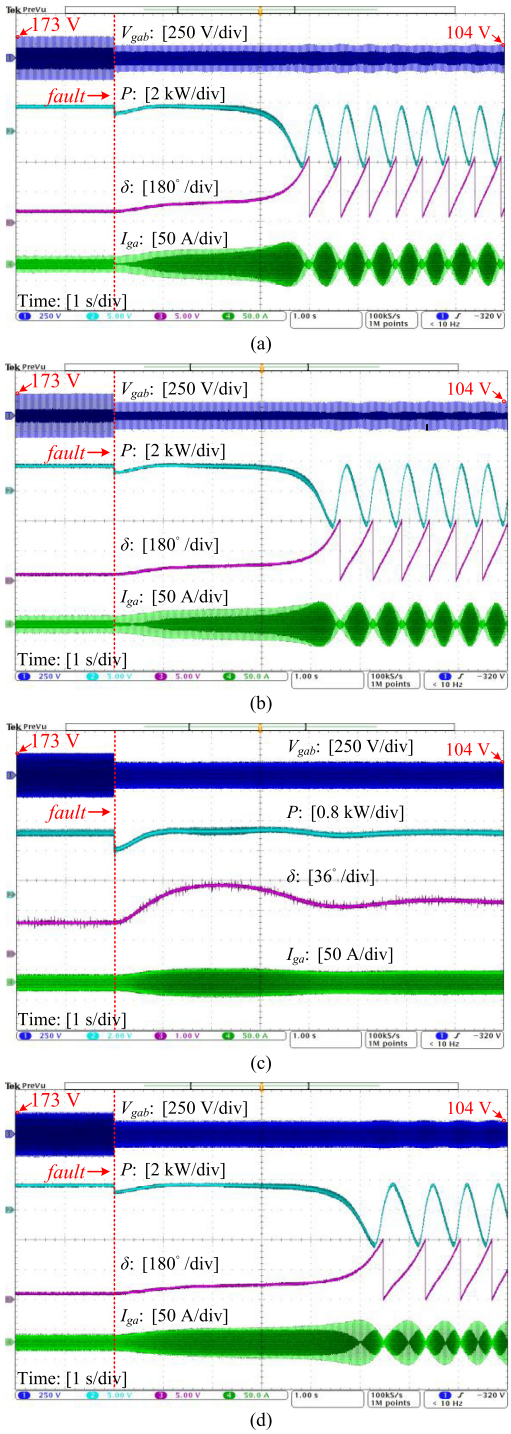

Fig. 6. Experimental transient responses of the VSG with different K_h of TDM ($\alpha = 3$ rad/s) when V_g dips from 1 to 0.6 p.u.: (a) without TDM ($K_h = 0$), (b) $K_h = 10$ p.u., (c) $K_h = 20$ p.u., and (d) $K_h = 60$ p.u.

and improve the transient stability due to the additional damping effect, i.e., $K_h = 20$ p.u. and $K_h = 50$ p.u. However, different from the conclusions from the small-signal stability, a too-large K_h will deteriorate the transient stability, such as $K_h = 60$ p.u. To solve this problem, the dynamics of HPF during the transient period should be considered.

It is reported that a positive D_p always supplies a positive damping effect to enhance transient stability [12]. Thus, x_1 in (3) always provides a positive damping effect. Then, x_2 is the root cause of negative impacts. Combining with Fig. 1, it can be concluded that the sign of x_2 should be the same as that of $\Delta\omega$, in order to provide a positive damping effect. Fig. 3(b) shows the trajectory projections on the $x_2 - \Delta\omega$ plane, which was divided into four regions by $x_2 = 0$ and $\Delta\omega = 0$. Almost all the trajectories belong to the second and fourth quadrants, which provide negative damping effects. Moreover, the impacts of x_2 become worse when K_h is increased, which can be clearly observed from the first stage of the trajectory, i.e., x_2 declines much more rapidly when K_h rises. As a result, $\Delta\omega$ even cannot decrease below zero when K_h increases to 60. To conclude, x_1 always supplies a positive damping effect, which can be improved by a larger K_h. Yet, x_2 has a negative influence, and it worsens more when K_h increases. Thus, K_h of the HPF needs to be chosen within a limited range of values to guarantee the transient stability of the system.

B. Design Guidelines of HPF

From the abovementioned analysis, the TDM can enhance synchronization stability with proper K_h and α selections. Thus, the allowable parameter ranges need to be found, which is also important design information for engineers to identify how far or close the system is from the instability region. To this end, many selections of α and K_h with a small change step need to be swept and examined. Substituting each set of α and K_h into (7) and then solve (7) with the command "ode45." According to the solutions, the dynamics of (7) can be checked whether stable or not under the specific set of α and K_h (if the solution of power angle δ exceeds δ_{ue} at any time, the system is unstable). In the beginning, a smaller number of selections is used to find the general parameter range, and then a large number of selections (such as 200×500 combinations in this letter) are examined to get more accurate results in our study. The computer used for the calculations is a Lenovo ThinkPad with a 1.99 GHz Intel Core i7-8550U processor, 24 GB of RAM, and a 64-bit operating system with Win10. Using this laptop, it requires about 10 min to test all 200×500 different combinations of α and K_h. Finally, after the large number selections of α and K_h are tested, the required parameter design space is specified automatically for transient stability, as shown in Fig. 4, where the stable and unstable operation regions are shaded and without shading, respectively. From there, it can be seen that α should be smaller than 3.3 rad/s. Otherwise, the TDM cannot enhance transient stability. With a smaller α, the allowable range for K_h becomes larger. However, the system dynamics will be slower. Therefore, $\alpha = 3$ rad/s is chosen in this letter, and K_h must be within [16 p.u., 54 p.u.], which agrees with the trajectory prediction in Fig. 3(a).

It should be noted that the detailed parameter design in Fig. 4 is conducted under the worst-case to guarantee the robust operation of the VSG with variations in grid impedance. Suppose the lowest short-circuit ratio of the grid is 2, the equivalent largest grid inductance can be calculated as 12 mH. Thus, the worst-case, i.e., $R_g = 0$ and $L_g = 12$ mH, is used to design the damping parameters, and the results are shown in Fig. 4. For a

much weaker grid, the analytical method and damping design guidelines established in this letter can be easily applied.

IV. Experimental Validation

The experimental setup, as shown in Fig. 5, is built to verify the theoretical analysis, and experiments are carried out in the lab. The main parameters of the VSG are given in Table I.

Fig. 6 shows the experimental transient responses of the VSG. It can be observed that without TDM, a low-frequency oscillation is triggered by the grid fault, which confirms the transient stability prediction by the trajectory in the state-space shown with the red line in Fig. 3(a). The instability can be removed by enabling the TDM with $K_h = 20$ p.u. in Fig. 6(c). However, if K_h is not large enough, i.e., $K_h = 10$ p.u., the TDM cannot provide an adequate damping effect during the transient period, still resulting in transient instability. Maintaining the K_h within its allowable range as determined by Fig. 4 to supply more damping effect, such as $K_h = 20$ p.u., the system can be stabilized. Yet, affected by the HPF dynamics, K_h cannot be too large. Otherwise, the system will lose synchronization again when K_h is increased to 60 p.u. These experimental results agree well with the theoretical analysis with the state-space trajectories depicted in Fig. 3 and the parameter range given in Fig. 4, which further confirms the correctness of the theoretical findings.

V. Conclusion

The effects of the TDM on transient stability are first studied in this letter. The state-space trajectories are adopted to illustrate that the TDM can enhance the power angle stability due to the more damping effects provided. However, influenced by the HPF dynamics, the parameters of TDM should be designed and chosen within a relatively limited range. The experimental results have verified the effectiveness of the theoretical analysis and the parameter range of TDM.

References

[1] J. Rocabert, A. Luna, F. Blaabjerg, and P. Rodriguez, "Control of power converters in ac microgrids," *IEEE Trans. Power Electron.*, vol. 27, no. 11, pp. 4734−4749, May 2012.

[2] Q. C. Zhong and G. Weiss, "Synchronverters: Inverters that mimic synchronous generators," *IEEE Trans. Ind. Electron.*, vol. 58, no. 4, pp. 1259–1267, Apr. 2011.

[3] T. Shintai, Y. Miura, and T. Ise, "Oscillation damping of a distributed generator using a virtual synchronous generator," *IEEE Trans. Power Del.*, vol. 29, no. 2, pp. 668–676, Apr. 2014.

[4] S. D. Arco, J. A. Suul, and O. B. Fosso, "A virtual synchronous machine implementation for distributed control of power converters in smartgrids," *Electr. Power Syst. Res.,* vol. 122, pp. 180−197, May 2015.

[5] O. Mo, S. D'Arco, and J. A. Suul, "Evaluation of virtual synchronous machines with dynamic or quasi-stationary machine models," *IEEE Trans. Ind. Electron.*, vol. 64, no. 7, pp. 5952−5962, Jul. 2017.

[6] J. A. Suul, S. D'Arco, and G. Guidi, "Virtual synchronous machine based control of a single-phase bi-directional battery charger for providing vehicle-to-grid services," *IEEE Trans. Ind. Appl.*, vol. 52, no. 4, pp. 3234–3244, Jul./Aug. 2016.

[7] S. Dong and Y. C. Chen, "Adjusting synchronverter dynamic response speed via damping correction loop," *IEEE Trans. Energy Convers.*, vol. 32, no. 2, pp. 608–619, Jun. 2017.

[8] J. Liu, Y. Miura, and T. Ise, "Fixed-parameter damping methods of virtual synchronous generator control using state feedback," *IEEE Access*, vol. 7, pp. 99177–99190, 2019.

[9] Y. Ma, W. Cao, L. Yang, F. Wang, and L. M. Tolbert, "Virtual synchronous generator control of full converter wind turbines with short term energy storage," *IEEE Trans. Ind. Electron.*, vol. 64, no. 11, pp. 8821–8831, Nov. 2017.

[10] L. Zhang, L. Harnefors, and H.-P. Nee, "Interconnection of two very weak AC systems by VSC-HVDC links using power-synchronization control," *IEEE Trans. Power Syst.*, vol. 26, no. 1, pp. 344−355, Feb. 2011.

[11] X. Xiong, and X. Ruan, "Non-smooth bifurcation analysis of multi-structure multi-operating-mode power electronics systems for applications with renewable energy sources," *IEEE Trans. Circuits Syst. II, Express Briefs*, vol. 66, no. 3, pp. 487–491, Mar. 2019.

[12] D. Pan, X. Wang, F. Liu, and R. Shi, "Transient stability of voltage-source converters with grid-forming control: A design-oriented study," *IEEE J. Emerg. Sel. Topics Power Electron.*, vol. 8, no. 2, pp. 1019–1033, Jun. 2020.

[13] H. Wu and X. Wang, "A mode-adaptive power-angle control method for transient stability enhancement of virtual synchronous generators," *IEEE J. Emerg. Sel. Topics Power Electron.*, vol. 8, no. 2, pp. 1034–1049, Jun. 2020.